Chinese Journal of Aeronautics, (2015), 28(4): 1296–1304

Chinese Society of Aeronautics and Astronautics
& Beihang University

Chinese Journal of Aeronautics

cja@buaa.edu.cn
www.sciencedirect.com

TEHL analysis of high-speed and heavy-load roller bearing with quasi-dynamic characteristics

Shi Xiujiang, Wang Liqin *

School of Mechatronics Engineering, Harbin Institute of Technology, Harbin 150001, China

Received 28 September 2014; revised 10 December 2014; accepted 12 March 2015
Available online 20 June 2015

KEYWORDS

Aero-engine mainshaft roller bearing;
Ellipticity;
Load;
Quasi-dynamics;
Radial clearance;
TEHL;
Velocity

Abstract In this paper, the aero-engine mainshaft roller bearing D1842926 under typical operating conditions is taken as a case study, a new integrated numerical algorithm of quasi-dynamics and thermal elastohydrodynamic lubrication (TEHL) is put forward, which can complete the bearing lubricated analysis from global dynamic performance to local TEHL state and break out of the traditional analysis way carried out independently in their own field. The 3-D film thickness distributions with different cases are given through integrated numerical algorithm, meanwhile the minimum film thickness of quasi-dynamic analysis, integrated numerical algorithm and testing are compared, which show that integrated numerical results have good agreements with the testing data, so the algorithm is demonstrated available and can judge the lubrication state more accurately. The parameter effects of operating and structure on *pv* value, cage sliding rate, TEHL film pressure, thickness and temperature are researched, which will provide an important theoretical basis for the structure design and optimization of aero-engine mainshaft roller bearing.

1. Introduction

Numerous studies of aeroengine mainshaft bearings have been undertaken due to the special operating conditions—high speed, heavy load and great heat,[1–6] which may lead to a sudden and catastrophic failure more easily than the common bearings. But with the development of bearing material, the main reason on bearing failure hardly comes from fatigue and more from the surface injure related to the lubrication state.[7]

In engineering practice, the film thickness ratio[8] is generally used to judge the lubrication state, thus the calculation accuracy of film thickness has a significant impact on the judgement of the lubrication state, particularly in the aero-engine mainshaft bearing which requires high reliability and precise limit design. But almost all the computations of minimum film thickness are obtained by fitting formulas in bearing dynamic analysis, and the most common one comes from Hamrock–Dowson (H–D)[9] whose minimum film thickness in general operating conditions agrees well with numerical results.[10,11] However, H–D formula at high speed and under heavy load conditions is limited on account of neglecting thermal effect, which had been proven by the previous researches of Luo[12]

* Corresponding author. Tel.: +86 451 8640 2012.
E-mail addresses: shixiujiang@163.com (X. Shi), lqwanghit@163.com (L. Wang).

Peer review under responsibility of Editorial Committee of CJA.

http://dx.doi.org/10.1016/j.cja.2015.06.013
1000-9361 © 2015 Production and hosting by Elsevier Ltd. on behalf of CSAA & BUAA.

and Sun et al.[13] Later, Wilson–Sheu[14] (W–S) came up with the modified formula with a modified factor on the basis of H–D's, which have been demonstrated to still have a large error in this paper because of not covering all the effects like bearing operation, structure, material, lubricant performance, etc. Besides, Lubrecht,[15] Canzi[16] and Zhu et al.[17] also pointed out the limitation of the fitting formulas and suggested the algorithm of numeric or testing should be adopted.

The numerical analysis[18,19] of thermal elastohydrodynamic lubrication (TEHL) is an effective and accurate algorithm for film thickness computation. But during the last years, the algorithm has been hardly connected with application engineering and has been used only for theoretical calculation of the single rolling element and the race. The elastohydrodynamic lubrication (EHL) analysis and the dynamic analysis are both carried out in their own field for the complicated calculation, which make the bearing numerical analysis become incomplete and inaccurate. So in this study the integrated numerical algorithm of aero-engine mainshaft roller bearing under typical operating conditions will be researched to provide an important theoretical basis for the judgement of lubrication state and structural optimization.

2. Governing equation

2.1. Force and motion analysis

The quasi-dynamic model with high accuracy and applicability is adopted, and the force equilibrium of the bearing and the roller is shown in Fig. 1. In which $OXYZ$ is the fixed coordinate system of the bearing and $O_{bj}x_ay_az_a$ is the follow-up coordinate system of the roller; j represents the jth roller, the roller is divided into n wafers, and k means the kth wafer; 1 and 2 represent the outer race and inner race; Q_{1jk} and Q_{2jk} mean the normal contact loads; T_{1jk} and T_{2jk} stand for the traction forces; P_{1jk} and P_{2jk} mean the film pressure; F_{cj} and f_{cj} are the normal and tangential forces of the cage; F_{dj} refers to the resistance of gas–oil mixture; F_{yj}, F_{zj} and M_{xj}, M_{yj}, M_{zj} are the initial forces and moments; F_x, F_y, F_z and M_y, M_z represent the applied forces and moments; Ψ_j ($j = 1,2,\ldots$) is the azimuth angle of the roller; ω_2 and ω_m, are the angular velocities of the inner race, the revolution of the cage; ω_{xj} and ω_{oj} are the rotation and the revolution of the roller. The quasi-dynamic equations' solution of cage and race can be obtained in Ref.[20] and the balanced equations are given in Eq. (1).

$$\begin{cases} \sum_{k=1}^{n}(T_{1jk}-T_{2jk}+P_{1jk}-P_{2jk})+F_{cj}+F_{dj}+F_{yj}=0 \\ \sum_{k=1}^{n}(Q_{2jk}-Q_{1jk})-f_{cj}+F_{zj}=0 \\ \frac{D_b}{2}\left[\sum_{k=1}^{n}(T_{2jk}+T_{1jk})-f_{cj}\right]+M_{xj}=0 \\ \sum_{k=1}^{n}(Q_{2jk}x_k-Q_{1jk}x_k)+M_{yj}=0 \\ \sum_{k=1}^{n}(P_{2jk}x_k-P_{1jk}x_k)+M_{zj}=0 \end{cases} \tag{1}$$

Fig. 2 presents the roller structure and the contact motion diagrams between the roller and the race. In which h_0 is the center film thickness of rigid bodies, R_x and R_y are the curvature radii of roller and modified roller radii (0.01 m), l is the total roller length and the straight length is $0.9l$, D_b is the roller diameter, ω_{bj} is the rotation of roller, x, y, z represent the directions of the rolling, the roller length and the film thickness. Assuming that outer race is fixed, the entrainment velocity U_{1j} and U_{2j} (average velocity of roller and outer/inner race), as well as the relative sliding velocity ΔU_{1j} and ΔU_{2j} are expressed as Eqs. (2)–(5), which can be solved through quasi-dynamic analysis.[20]

$$U_{1j}=\frac{D_m}{4}\left[(1+\gamma')\omega_m+\gamma'\omega_{bj}\right] \tag{2}$$

$$U_{2j}=\frac{D_m}{4}\left[(1-\gamma')(\omega_2-\omega_m)+\gamma'\omega_{bj}\right] \tag{3}$$

$$\Delta U_{1j}=\frac{D_m}{2}\left[(1+\gamma')\omega_m-\gamma'\omega_{bj}\right] \tag{4}$$

$$\Delta U_{2j}=\frac{D_m}{2}\left[(1-\gamma')(\omega_2-\omega_m)-\gamma'\omega_{bj}\right] \tag{5}$$

where γ' is defined as D_b/D_m, and D_m is the bearing pitch diameter.

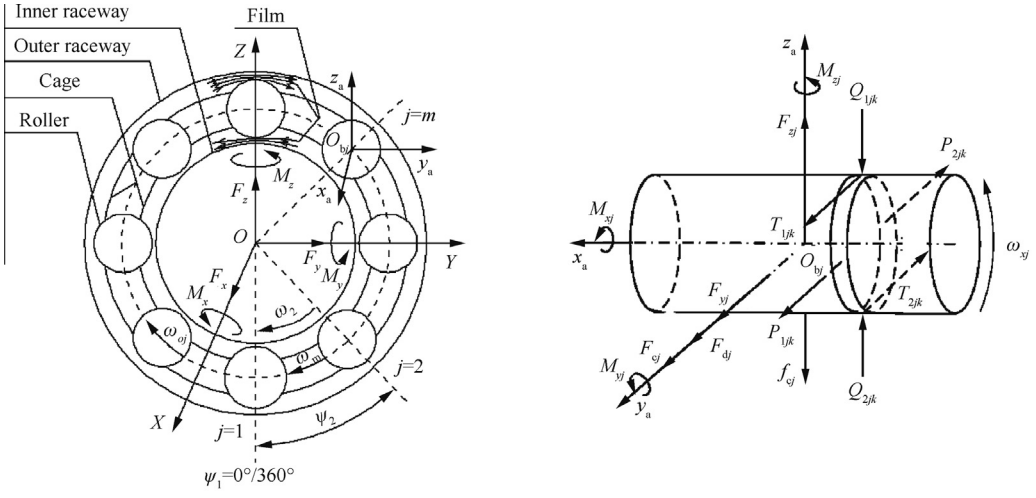

(a) Force of bearing (b) Force of roller

Fig. 1 Force equilibrium of bearing and roller.

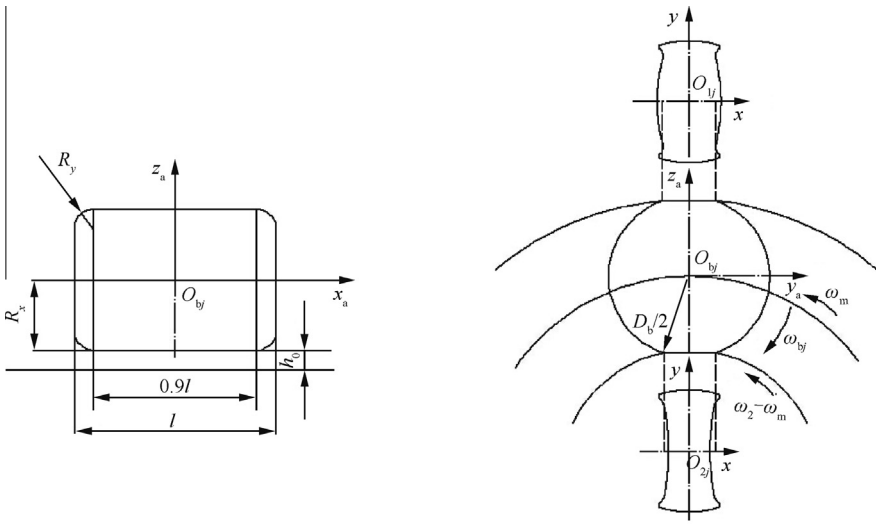

(a) Roller structure (b) Contact motion state of roller and races

Fig. 2 Roller structure and contact motion state of roller and races.

2.2. TEHL equations

The difference between thermal and isothermal Reynolds[21] equation is the density and viscosity of TEHL varying in the film thickness direction. But the equation format is similar, only ρ/η and ρ are replaced by $(\rho/\eta)_e$ and ρ^*, which can be reduced to the following form:

$$\frac{\partial}{\partial x}\left[\left(\frac{\rho}{\eta}\right)_e h^3\frac{\partial p}{\partial x}\right]+\frac{\partial}{\partial y}\left[\left(\frac{\rho}{\eta}\right)_e h^3\frac{\partial p}{\partial y}\right]=12U_{2j}\frac{\partial(\rho^* h)}{\partial x} \tag{6}$$

where p and h are the film pressure and thickness, η and ρ are the film viscosity and density, and the density/viscosity–pressure–temperature equations come from Ref.[22]; $(\rho/\eta)_e$ and ρ^* are defined as

$$\begin{cases}(\rho/\eta)_e=12(\eta_e\rho'_e/\eta'_e-\rho''_e)\\ \rho^*=2(\rho_e-\eta_e\rho'_e)\end{cases}$$

where η_e, η'_e, ρ_e, ρ'_e, ρ''_e can be obtained by

$$\begin{cases}\eta_e=h/\int_0^h\frac{\mathrm{d}z}{\eta}\\ \eta'_e=h^2/\int_0^h\frac{z\mathrm{d}z}{\eta}\\ \rho_e=\frac{1}{h}\int_0^h\rho\mathrm{d}z\\ \rho'_e=\frac{1}{h^2}\int_0^h\rho\int_0^z\frac{\mathrm{d}z'}{\eta}\mathrm{d}z\\ \rho''_e=\frac{1}{h^3}\int_0^h\rho\int_0^z\frac{z'\mathrm{d}z'}{\eta}\mathrm{d}z\end{cases}$$

The film thickness equation taking elastic deformation into account is calculated by

$$h(x,y)=h_0+\frac{x^2}{2R_x}+\frac{(|y|-0.9l)^2}{2R_y}f-\frac{2}{\pi E'}\frac{p(x',y')}{\sqrt{(x-x')^2+(y-y')^2}}\mathrm{d}x'\mathrm{d}y' \tag{7}$$

where E' is the general elastic modulus and the forth term in the equation represents the elastic deformation of a point (x',y') under the pressure $p(x',y')$.

The energy equation of the film can be expressed in the form

$$c_0\left[\rho u\frac{\partial T}{\partial x}+\rho v\frac{\partial T}{\partial y}-q\frac{\partial T}{\partial z}\right]-k_0\frac{\partial^2 T}{\partial z^2}=-\frac{T}{\rho}\cdot\frac{\partial\rho}{\partial T}\left(u\frac{\partial p}{\partial x}+v\frac{\partial p}{\partial y}\right)+\eta\left(\left(\frac{\partial u}{\partial z}\right)^2+\left(\frac{\partial v}{\partial z}\right)^2\right) \tag{8}$$

where z is the coordinate along film thickness direction, c_0 and k_0 are the film specific heat and thermal conductivity, u and v are the flow velocities along x and y axis, and q is flow of the lubricant.

3. Numerical analysis method

Fig. 3 presents the basic solving steps. First, the initial conditions are given, which take the H–D's minimum film thickness as the starting film thickness, then the quasi-dynamic equations are solved to get the micro-contact field motion and stress state by Newton–Raphson and steepest descent methods.[20] Further, TEHL analysis is conducted to acquire the EHL performance including film thickness, pressure and temperature. In the solving process of TEHL analysis, the lubrication equations are dimensionlessed, dispersed[22] and solved by multi-grid method. The grids employed to solve film pressure include 5 layers, which have 128 nodes in x direction and 1024 nodes in y direction on the top layer. And the column-scan method is used to solve thermal field whose grid number is the same as that in the top layer of pressure solution; the nodes in film thickness direction contain each 6 nodes in the bodies and 10 nodes in the film.

4. Results and discussion

4.1. Minimum film thickness comparison with different algorithms

The basic parameters of aeroengine mainshaft roller bearing D1842926 and aero lubricant 4109 are given in Tables 1 and 2.

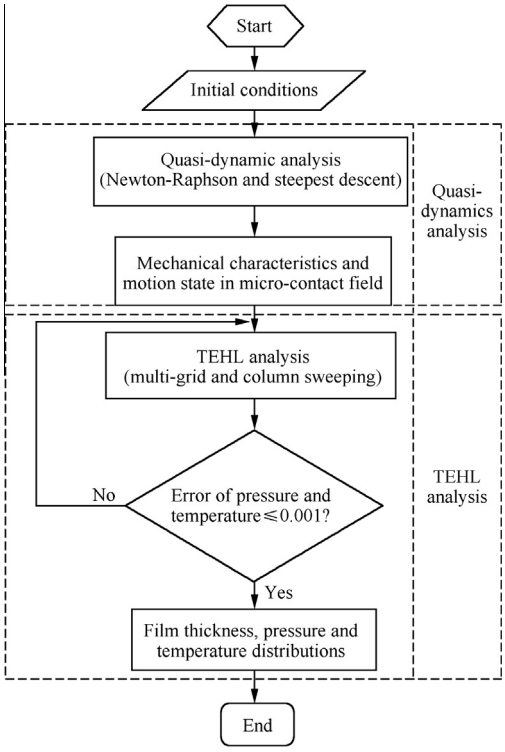

Fig. 3 Flow diagram of numerical analysis.

Table 1 Basic parameters of aeroengine mainshaft roller bearing D1842926.[23]

Material parameter	Value	Geometry parameter	Value
Elastic modulus of roller and race (GPa)	218	Inner radius (mm)	130
Poisson's ratio of roller and race	0.3	Outer radius (mm)	180
Density of roller and race (kg/m^3)	7870	Roller diameter (mm)	12
Elastic modulus of cage (GPa)	209	Total roller length (mm)	12
Poisson's ratio of cage	0.3	Straight roller length (mm)	10.8
Density of cage (kg/m^3)	7870	Roller number	30
Specific heat (J/(kg·°C))	460	Thermal conductivity (N/(s·°C))	15

Table 2 Basic parameters of aero lubricant 4109.

Parameter	Value	Parameter	Value
Environmental viscosity (Pa·s)	0.033	Viscosity–temperature coefficient (°C^{-1})	0.032
Environmental density (kg/m^3)	970	Viscosity–pressure coefficient (Pa^{-1})	1.85×10^{-8}
Specific heat (J/(kg·°C))	1910	Thermal conductivity (N/(s·°C))	0.0966

Since the outer race radii is larger than the inner race one, which means the relative velocity of the out race is larger, the film forms easier in the outer race and the minimum film thickness would appear in the micro-contact field of the inner race and the rollers. In quasi-dynamic analysis, the minimum film thickness use to be calculated by fitting formulas. Fig. 4 shows the contact operating conditions (contact load and entrainment velocity) in micro-contact field between rollers and inner race which are obtained by quasi-dynamic analysis under 4 cases from Ref.[23]. The applied radial loads of the 4 cases are 8 kN, 12 kN, 18 kN and 24 kN, and the velocities of the inner race are all 13218 r/min. As seen in Fig. 4, the contact loads and the loaded roller number increase with the increasingly applied radial load, and the entrainment velocities almost keep unchanged because of the same inner race velocities.

The integrated numerical analysis of quasi-dynamics and TEHL is put forward in this paper. The minimum film thicknesses all appear at the 360° azimuth angle of the roller, which is caused by the maximum load at this location, and the 3-D film thickness distributions in 4 cases are provided in Fig. 5, which reveals that the minimum film thicknesses are 0.514 μm, 0.490 μm, 0.471 μm and 0.445 μm, and b represents the half width of Hertz contact. As can be seen in Fig. 5, the minimum film thicknesses emerge on both sides of the roller for the stress concentration, which becomes more and more apparent from Case1 to Case 4 due to the increasing load.

At the same time, the minimum film thickness distributions between the inner race and rollers from Case 1 to Case 4 with 4 methods are described in Fig. 6, which indicate that H–D's minimum film thickness has a large error due to neglecting thermal effect, though the error of W–S's decreases, which is still above 40% for not covering all the testing conditions such as bearing operating, structure, material, lubrication parameters, etc. The numerical results have a great agreement with the testing results[23] whose error is only within 10%, which prove that the algorithm is available and can judge the lubrication state more accurately.

4.2. Operating condition effects on bearing tribology performance

4.2.1. Radial load effects

Above all, thermal effect has a large influence on the film thickness. In bearing dynamic analysis, the cage sliding ratio defined as the ratio of the difference between the actual cage velocity and the theoretical velocity to the theoretical velocity and the pv value represented as the product of the contact stress and the relative sliding velocity between the rollers and the inner race are often used to characterize heat distribution, and the larger the cage sliding ratio and the pv value, the more the heat.

As the rollers and inner race contact, the distributions of cage sliding ratios and the pv values under different applied radial loads (the velocity are all 13218 r/min) are shown in Fig. 7, which suggests that the cage sliding ratio decreases with the increase of the load. The loaded rollers increase with the increase of the load, which causes the cage velocity to increase and the sliding ratio decreases. However, the pv values increase from 8 kN to 12 kN and decrease from 12 kN to 18 kN. The reasons are that the loaded rollers keep the same from 8 kN to 12 kN firstly, the high load leads to high pressure, so the pv values increase; then, the loaded rollers increase with the

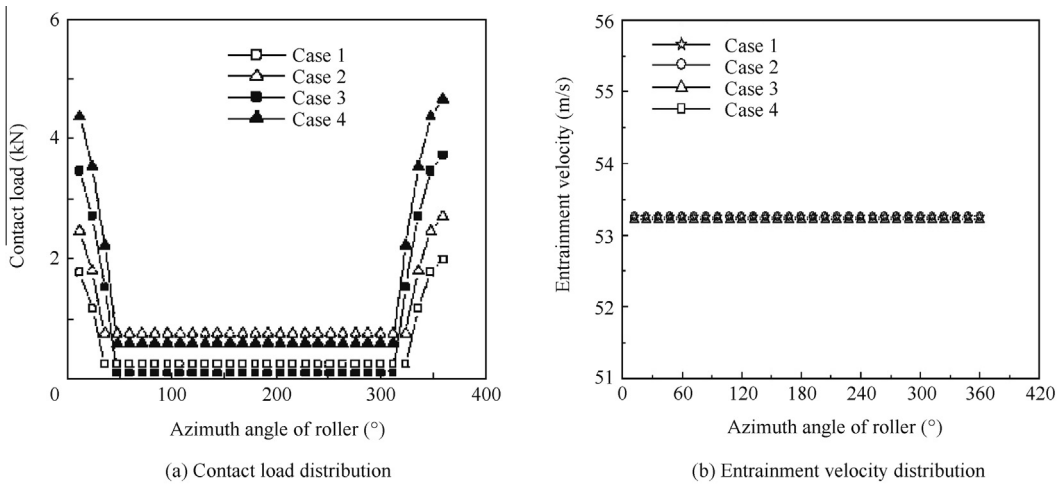

(a) Contact load distribution (b) Entrainment velocity distribution

Fig. 4 Contact load and entrainment velocity in micro-contact field between rollers and inner race.[23]

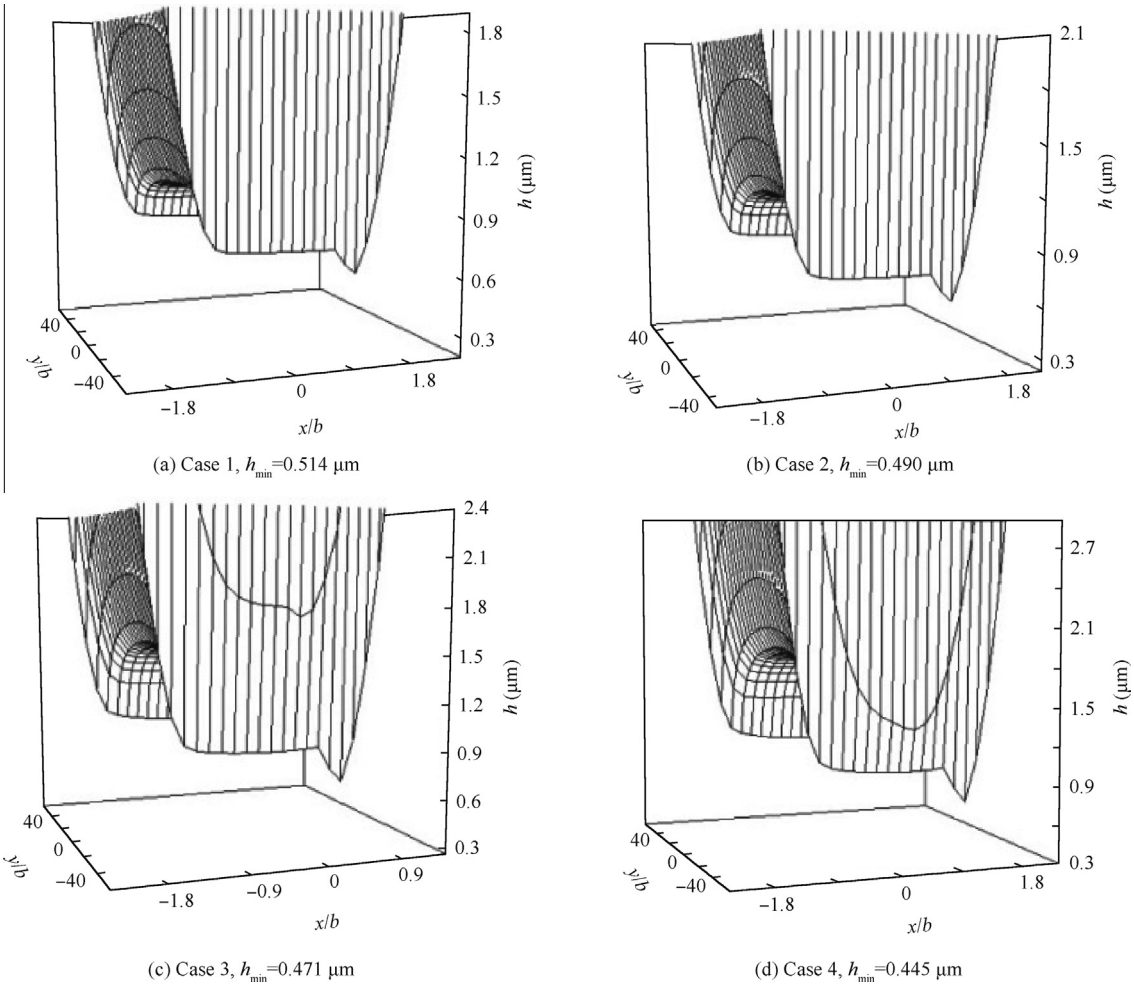

(a) Case 1, h_{min}=0.514 μm (b) Case 2, h_{min}=0.490 μm

(c) Case 3, h_{min}=0.471 μm (d) Case 4, h_{min}=0.445 μm

Fig. 5 3-D film thickness distributions in different cases.

increasing load from 12 kN to 18 kN, the pressure of the single roller decreases, and the *pv* values decrease.

Meanwhile, Fig. 8 presents the distributions of dimensionless film pressure, thickness and temperature with different applied radial loads (the velocities are all 13218 r/min) in the rolling direction at 360° azimuth angle of the roller through the integrated numerical algorithm, where $\bar{p}$ is the dimensionless film pressure, $\bar{h}$ the dimensionless film thickness, and $\overline{T}$ the dimensionless film temperature, $\bar{x}$ the dimensionless coordinate in the half width direction of Hertz contact. As shown in Fig. 8, with increasing stress and friction heat the pressure and the temperature increase, and the film thickness decreases.

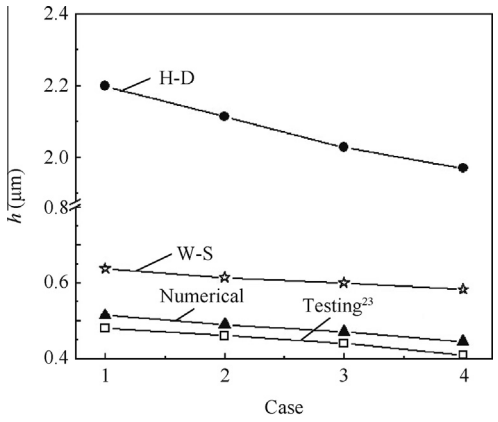

Fig. 6 Minimum film thickness distributions with four methods.

4.2.2. Velocity effects

Fig. 9 displays the distributions of cage sliding ratios and the *pv* values at different velocities (the loads are all 18 kN), which shows that the cage sliding ratios increase with the increase of the velocity. Since the loaded field decreases with the increasing centrifugal force caused by the increase of the velocity, which make the cage velocity decrease and the sliding ratios increase. And the *pv* values increase with the increase of the velocity, because the relative velocity increases with the increasing velocity, which leads the *pv* values to increase.

Further, the distributions of dimensionless film pressure, thickness and temperature at different velocities (the load are all 18 kN) are portrayed in Fig. 10, which states that the pressures are almost the same, the temperature increases because of the increasing relative sliding velocity which increases with the increase of the velocity and the film thickness increases with the increase of fluid hydrodynamic effect.

4.3. Structure effects

4.3.1. Radial clearance effects

Take Case 4 as an example, the distributions of cage sliding ratios and the *pv* values under different radial clearance (the ellipticity is 0) are depicted in Fig. 11, which shows the cage sliding ratios and the *pv* values increase with the increase of the radial clearance. Since the loaded roller number decreases with the increase of the radial clearance, which makes the cage sliding ratios increase, the contact stress and the relative velocity increase and the *pv* values increase.

In the meantime, Fig. 12 gives the distributions of dimensionless film pressure, thickness and temperature under different radial clearance (the ellipticity is 0), which shows that the pressure and the temperature increase on account of the increasing relative sliding velocity and the stress with the increase of the radial clearance, and the film thickness decreases.

4.3.2. Ellipticity effects

Fig. 13 displays the cage sliding ratio and the *pv* value distributions under different ellipticity (the radial clearance is 60 μm), which indicates the sliding ratios and the *pv* values decrease with the increase of ellipticity. As the ellipticity exists, the mainshaft will be forced more times during a rotation period,

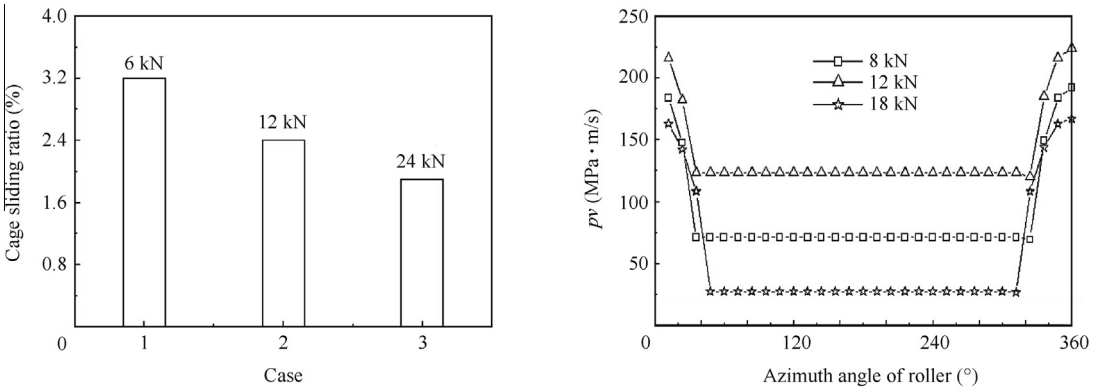

(a) Radial load effects on sliding ratio (b) Radial load effects on *pv* value

Fig. 7 Radial load effects on cage sliding ratio and *pv* value.

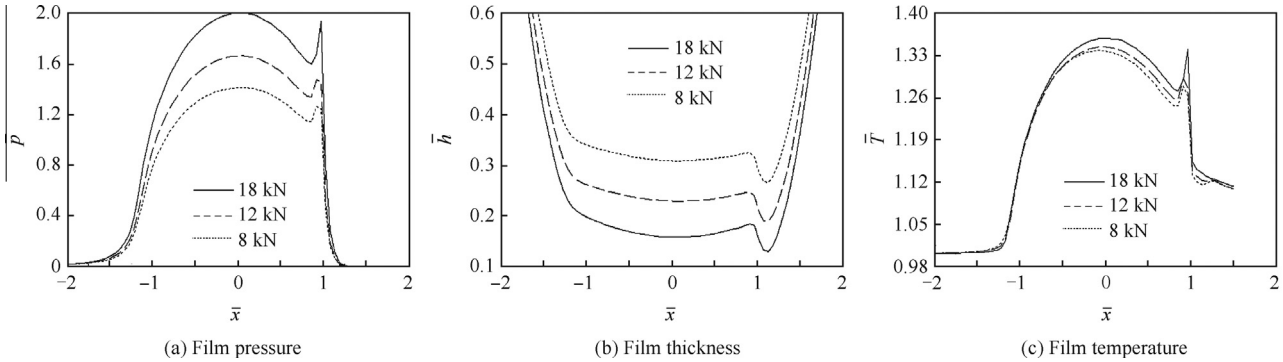

(a) Film pressure (b) Film thickness (c) Film temperature

Fig. 8 Radial load effects on film pressure, thickness and temperature.

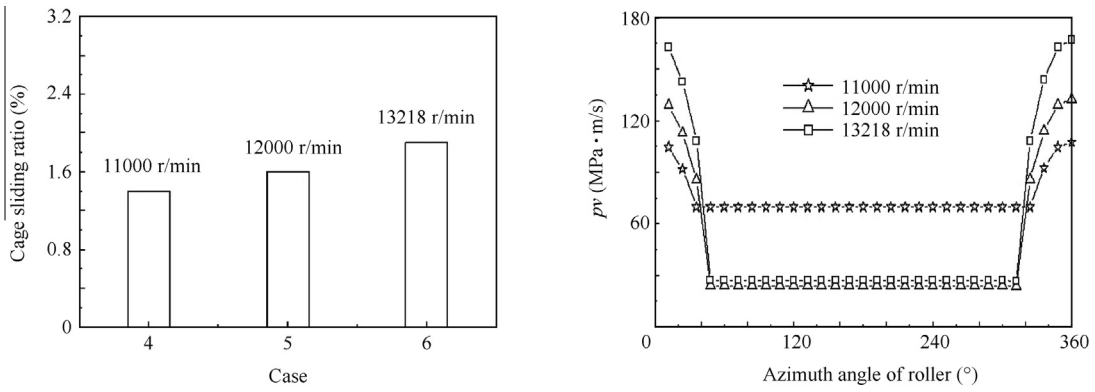

(a) Velocity effects on cage sliding ratio (b) Velocity effects on *pv* value

Fig. 9 Velocity effects on cage sliding ratio and *pv* value.

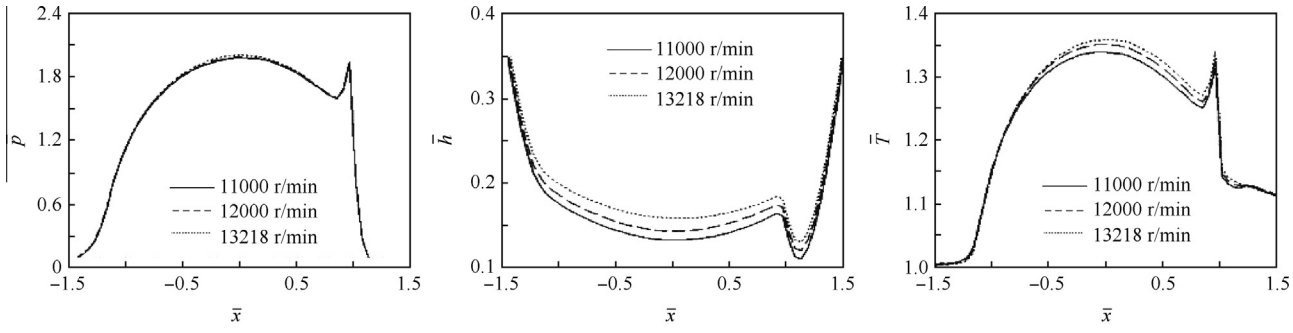

(a) Film pressure (b) Film thickness (c) Film temperature

Fig. 10 Velocity effects on film pressure, thickness and temperature.

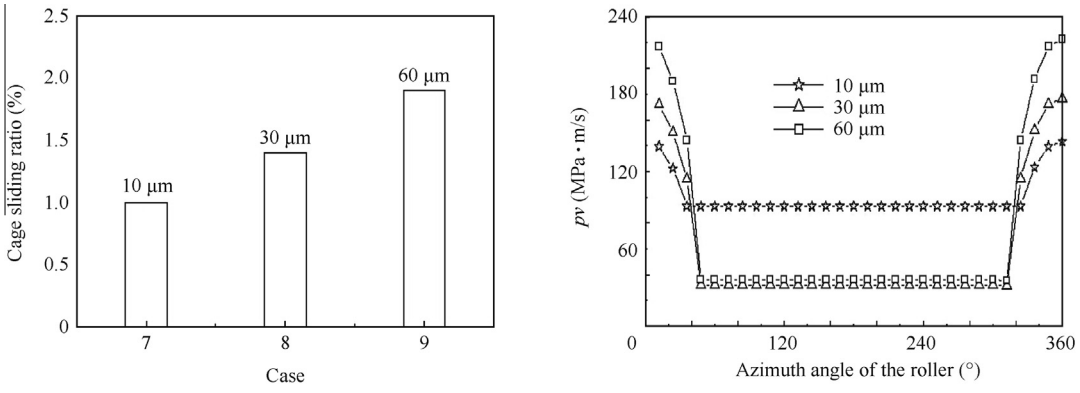

(a) Radial clearance effects on cage sliding ratio (b) Radial clearance effects on *pv* value

Fig. 11 Radial clearance effects on cage sliding ratio and *pv* value.

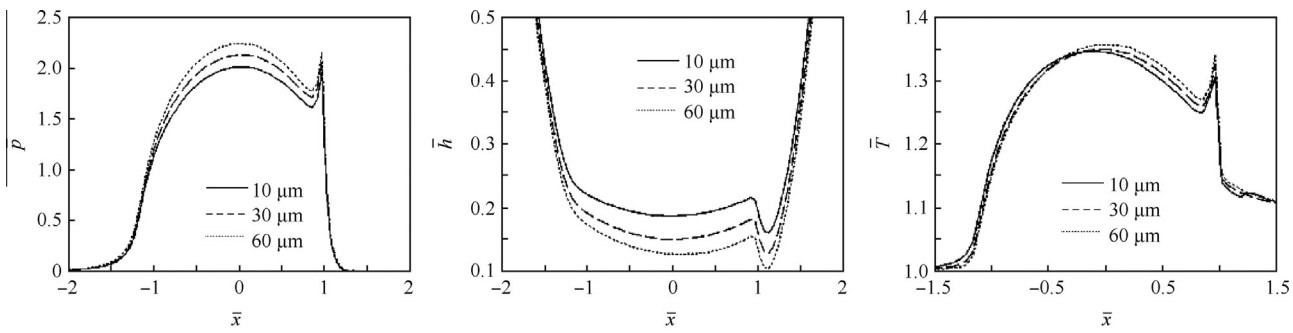

(a) Film pressure (b) Film thickness (c) Film temperature

Fig. 12 Radial clearance effects on film pressure, thickness and temperature.

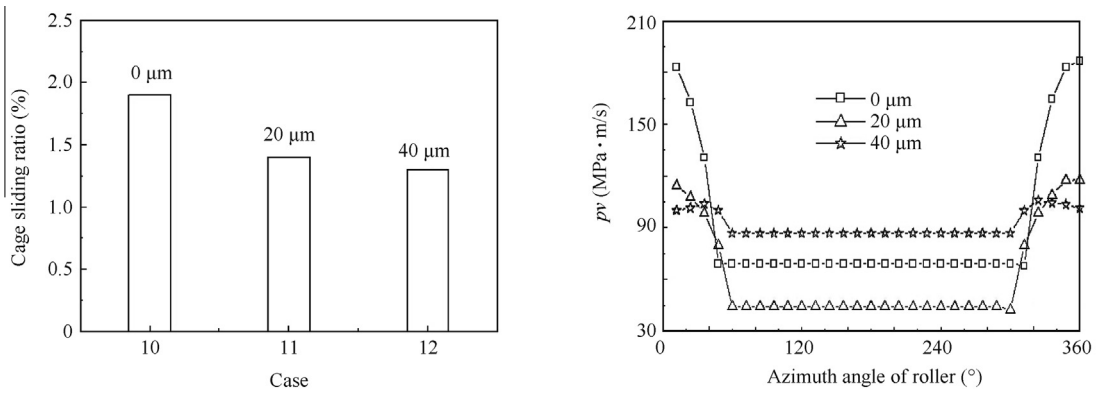

Fig. 13 Ellipticity effects on cage sliding ratio and *pv* value.

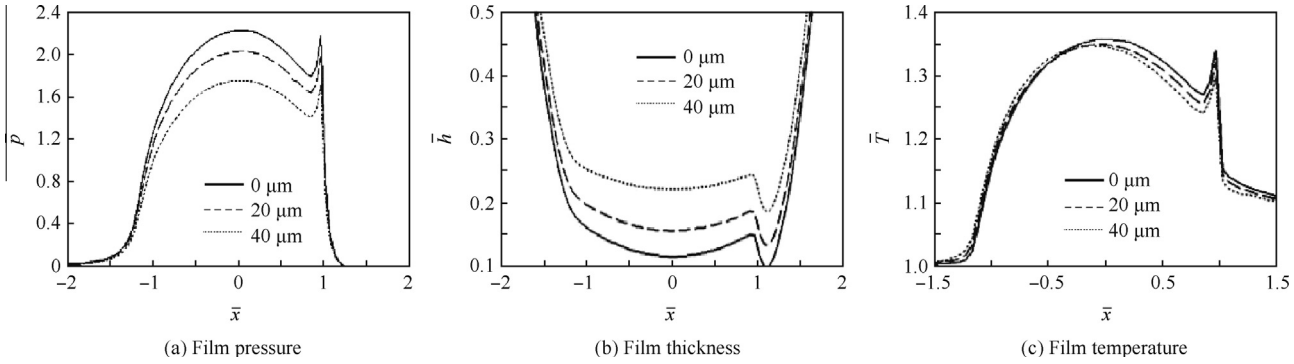

Fig. 14 Ellipticity effects on film pressure, thickness and temperature.

which means the more rollers will be preloaded, the loaded rollers will increase, the cage sliding ratio will decrease, the contact stress and the relative velocity will decrease, which will lead *pv* values to decrease.

Furthermore, the distributions of dimensionless film pressure, thickness and temperature under different ellipticity[24] (the radial clearance is 60 μm) defined as the distance of raceway and base circle are shown in Fig. 14, which declares that the pressure and the temperature decrease with the increase of ellipticity and the film thickness increases. This is caused by the decreasing relative sliding velocity and pressure with the increase of ellipticity; the temperature decreases, the contact load decreases and the film thickness increases.

5. Conclusions

(1) The 3-D film thickness distributions with different cases are given through integrated analysis and the minimum film thickness of quasi-dynamic analysis and integrated analysis are compared. Results show that the integrated numerical minimum film thicknesses are closer to the testing results, which prove that the integrated analysis is available and can be used to judge the lubrication state more accurately.

(2) The effects of operating conditions on bearing tribology performance are researched, which indicate that the cage sliding ratios decrease with the increasing loads, the *pv* values increase firstly then decrease; the film pressure and the temperature increase, and the thickness decreases. The cage sliding ratios and *pv* values increase with the increase of the velocity, the film pressure almost keeps the same, and the temperature and the thickness increase.

(3) The influences of structural conditions on bearing tribology performance are discussed, which claim that the cage sliding ratios and *pv* values increase with the increase of the radial clearance; the film pressure and the temperature increase; the thickness decreases. The cage sliding ratios and *pv* values decrease with the increasing ellipticity, the film pressure and the temperature decrease, and the thickness increases.

Acknowledgments

This study was supported by the National Key Basic Research Program of China (No. 2013CB632305) and the National Natural Science Foundation of China (No. 51373186).

References

1. Wang LQ, Cui L, Zheng DZ, Gu L. Analysis on dynamic characteristics of aero-engine high-speed ball bearings. *Acta Aeronautica et Astronautica Sinica* 2007;**28**(6):1461–7 [Chinese].
2. Sakaguchi T, Harada K. Dynamic analysis of cage behavior in a tapered roller bearing. *J Tribol* 2006;**128**(3):604–11.
3. Hu X, Luo GH, Gao DP. Quasi-static analysis of cylindrical roller intershaft bearing. *J Aerosp Power* 2006;**21**(6):1069–74 [Chinese].
4. Cui L, Wang LQ, Zheng DZ, Gu L. Analysis on dynamic characteristics of aero-engine high-speed roller bearings. *Acta Aeronautica et Astronautica Sinica* 2008;**29**(2):492–8 [Chinese].

5. Deng SE, Fu JH, Wang YS, Yang HS. Analysis on dynamic characteristics of aero-engine rolling bearing/dual-rotor system. *J Aerosp Power* 2013;**28**(1):195–204 [Chinese].
6. Ye ZH. Research on dynamic behavior of high-speed rolling bearing in aeroengines [dissertation]. Harbin: Harbin Institute of Technology; 2013 [Chinese].
7. Chen GC. Thermal analysis of high-speed rolling bearing used in mainshaft of aero-engine [dissertation]. Harbin: Harbin Institute of Technology; 2008 [Chinese].
8. Liu JY, Tallian TE, McCool JI. Dependence of bearing fatigue life on film thickness to surface roughness ratio. *ASLE Trans* 1975;**18**(2):144–52.
9. Hamrock BJ, Dowson D. Isothermal elastohydrodynamic lubrication of point contacts, Part III—fully flooded results. *ASME J Lubr Technol* 1977;**99**(2):261–76.
10. Guo K, Yuan SH, Zhang YY, Wang XL. Study on the calculation method of ball bearing mechanical characteristics considering elastohydrodynamic lubrication with spinning. *J Mech Eng* 2013;**49**(15):62–7.
11. Chen FH, Wang JG, Zhang GY. Elastohydrodynamic lubrication of tapered roller with logarithmic profile. *J Mech Eng* 2011;**47**(19):143–8.
12. Liang H, Guo D, Luo JB. Experimental investigation and numerical results comparison of elastohydrodynamic (EHD) film thickness behavior at high speeds. *Proceedings of the 11th national tribology conference*; 2013 Aug 6–9; Lanzhou, China. Beijing: CMES; 2013. p. 1–3 [Chinese].
13. Sun HY, Zhang YP, Guan DZ, Zhang PG. Study on the suitability for the Hamrock–Dowson formula under heavy load and high speed working conditions. *J Qingdao Univ* 2011;**26**(3):82–5 [Chinese].
14. Wilson WRD, Sheu S. Effect of inlet shear heating due to sliding on elastohydrodynamic film thickness. *Trans ASME* 1983;**105**(2):187–8.
15. Lubrecht AA, Venner CH, Colin F. Film thickness calculation in elastohydrodynamic lubricated line and elliptical contacts. *J Eng Tribol* 2009;**223**(3):511–5.
16. Canzi A, Venner CH, Lubrecht AA. Film thickness prediction in elastohydrodynamically lubricated elliptical contact. *J Eng Tribol* 2010;**224**(9):917–23.
17. Zhu D. Elastohydrodynamic lubrication in extended parameter ranges—Part II: load effect. *Tribol Trans* 2002;**45**(4):549–55.
18. Yin CL, Yang P. Analysis of oil supply conditions for EHL on elliptical contacts. *Tribology* 2007;**27**(2):147–51 [Chinese].
19. Pu W, Wang JX, Zhu D, et al. Semi-system approach in elastohydrodynamic lubrication of elliptical contacts with arbitrary entrainment. *J Mech Eng* 2014;**50**(13):106–12.
20. Cui L. Research on dynamic performances of high-speed rolling bearing and rotor system of aeroengine [dissertation]. Harbin: Harbin Institute of Technology; 2008 [Chinese].
21. Yang P, Wen S. A generalized Reynolds equation for non-Newtonian thermal elastohydrodynamic lubrication. *ASME J Tribol* 1990;**112**(4):631–6.
22. Liu XL, Yang PR. Analysis for finite line contacts of thermal elastohydrodynamic lubrication. *Tribology* 2002;**22**(4):296–9 [Chinese].
23. Zhang PS, Zhai WJ, Zhan MX, Shao JX, Wang HQ, Xiao BQ. Aeroengine elastohydrodynamic lubrication research on three typical spindle bearing. *Proceedings of the 11th national tribology conference*; 1992 Aug 6–9; Wuhan, China. Beijing: CMES; 992. p. 322–6 Chinese].
24. Wang LQ, Chen GC. Pre-deformation machining technology of the noncircular raceway of aero roller bearings. *Chin J Mech Eng* 2005;**41**(9):223–7 [Chinese].

Shi Xiujiang is a Ph.D. student at the School of Mechatronics Engineering, Harbin Institute of Technology. He received the B.S. and M.S. degrees in mechanical engineering from Qingdao Technological University in 2011 and 2014 respectively. His area of research includes rolling bearing dynamics and TEHL.

Wang Liqin is a professor and Ph.D. supervisor at the College of Mechatronic Engineering, Harbin Institute of Technology. His current research interests are aerospace tribology and rolling bearing of high performance.